A STUDY OF MITR--II CORE TANK AGING FOR RELICENSING CONSIDERATION

by

JYH-TZONG HWANG

Course 22.39

" Nuclear Reactor Operations And safety "

December 9, 1992

Massachusetts Institute of Technology

Abstract

A program to upgrade and to obtain approval for extending the operating life of the Massachusetts Institute of Technology Research Reactor (MITR) is undergoing. In order to extend the life of the reactor, it is essential to predict the remaining life of various components of the plant. Each components and systems of the reactor plant play their particular role in the safety and/or reliability function of the plant. They are also subject to the age-related degradation for the service environments. The structure integrity of the core tank is essential for ensuring that the reactor core will remain stable during normal operation, anticipated transient, and emergency and faulted condition. The purpose of this report is to assess, based on currently available experimental information, the suitability of the reactor core tank for extended operation at higher power level

Table of Contents

List of Figures

List of Tables

I Introduction

A program to upgrade and to obtain approval for extending the operating life of the Massachusetts Institute of Technology Research Reactor MITR) is undergoing. In order to extend the life of the reactor, it is essential to predict the remaining life of various components of the plant. Each components and systems of the reactor plant play their particular role in the safety and/or reliability function of the plant. They are also subject to the age-related degradation for the service environments. Aging of components and materials refers to the variation of their properties with time, the properties of interest being those related to the safety function of the component or material.

The structure integrity of the core tank is essential for ensuring that the reactor core will remain stable during normal operation, anticipated transient, and emergency and faulted condition. The reactor core tank is subject to age-related degradation for the reactor coolant environments, particularly from neutron irradiation. The purpose of this report is to assess, based on currently available experimental information, the suitability of the reactor core tank for extended operation at higher power level. Section II of the report provides general description of the Massachusetts Institute of Technology Research Reactor. Section III will discuss the aging mechanisms of the core tank material (aluminum 6061 alloy), and Section IV will evaluate the suitability of the core tank for extended operation. Finally, the conclusions and recommendations will be presented in Section V.

II Description of MITR--II

The original Massachusetts Institute of Technology Reactor, MITR-I, was both heavy-water moderated and cooled with an open array of plate-type fuel elements. This original core attained criticality in July 1958 and operated at power levels of up to five megawatts until 1974. The present core, MITR--II, is a heavy-water reflected, light-water cooled and moderated nuclear reactor which utilizes flat, plate-type, finned, aluminum-clad fuel elements highly enriched (93%) in U-235. The reactor is designed to operate at power levels of five megawatts. The operating temperature and pressure are 40 to 53 °C and atmospheric with hydrostatic pressure from twelve inches of H_2O, respectively. A vertical cross-section of the MITR-II depicting both major components and experimental facilities is shown in Figure 1 and 2 [1].

The reactor core is centered within three concentric metal vessels each of which provides protection to the core against loss of coolant and can be considered as a containment barrier. The outermost tank, which is made of steel, serves as a liner between the biological shield and, moving radially inward, a two feet thick graphite annulus that functions as a reflector. Both the concrete shield and graphite reflector contain penetrations for various experimental facilities such as the beam ports, the fast blanket, the medical room shutters etc.

The reflector tank, which is four feet in diameter, is used to maintain the heavy water at the level necessary for reactor operation. The D_2O system includes a pump and heat exchanger to dissipate heat generated in the heavy water and a dump tank for rapid reduction of reactivity by lowering the D_2O level. This capability serves as a backup emergency method for reactor shutdown. The heavy-water reflector is a closed system. This is important so as to avoid both the degradation of the heavy water and the release of tritium which is formed whenever a neutron is absorbed by deuterium oxide. The D_2O reflector tank is constructed of high purity aluminum 6061 alloy. The lower part of this tank has an inside diameter of 47.25 inches with a wall thickness of 0.375 inches. It expands at the top to an inside diameter of 54.75 inches. Its overall height is 122 inches .

The innermost of the three tanks is constructed of high purity aluminum 6061 alloy vessel of varying diameter that is referred to as the core tank. It contains the light water that cools and moderates the reactor core. The bottom section of the tank has three diameter transitions. The bottom portion has an inside diameter of twenty-inches. It then widens to an inside diameter of forty-five inches with a wall thickness of 0.25 inches and finally to an inside diameter of fifty inches with a wall thickness of one inch. An elevated support ring, which supports the core support housing assembly and the core shroud, is welded to the bottom of the forty-five inch diameter section. Immediately below the top flange of the core tank is the eight-inch primary coolant inlet pipe that leads to the inlet plenum. The over-all height of the core tank bottom section from the dished bottom to the top flange, is 102.375 inches. The tank's design pressure is 24 psig. The top section of the core tank has an inside diameter of forty-four inches with a wall thickness of 0.75 inches and overall height of fifty inches. Its diameter matches that of the top flange of the bottom section of the tank.

Surrounding the tank, nineteen inches below the top lip, are six penetrations, sixty degrees apart, for the shim blade drive mechanism and one penetration for the regulation

rod drive. The regulation rod is on the center-line of the thermal column. Penetrations also exist for the tank level probe and pressure taps.

Energy released by the fission of U-235 is removed by forced convection. The light-water coolant that enters the tank from the inlet plenum is directed to the annulus formed by the flow shroud and the tank's inner wall. It then flows downward through this annulus, under the support ring, and through another annulus formed by the core tank and housing until reaching the bottom of the fuel assemblies. It is then directed upward through the fuel elements and into the large outlet plenum above the core. The energy removed from the core is transferred through three heat exchangers to the secondary coolant system whereupon it is dumped to the atmosphere via two cooling towers. The use of a secondary coolant system is important as it allows the reactor's heat to be dissipated while maintaining the slightly radioactive primary coolant in a closed loop.

Two anti-syphon valves are positioned at the upper junction of the flow shroud and the core tank. These, together with four natural convection valves that are located on the support ring are held closed by primary pump pressure and will open automatically if flow is lost. The former are intended to prevent siphoning of water out of the core tank should a primary inlet pipe rupture. The function of the latter is to promote natural circulation cooling if both the normal and emergency electric power supplies should be lost.

III Aluminum 6061 Alloy Aging Mechanisms

Aluminum 6061 alloy is an age-hardenable alloy. Figure 3 shows the aging characteristics of the alloy [3]. The chemical composition limits of aluminum 6061 alloy used in nuclear reactor applications is shown in Table 1 [2]. The typical physical, thermal, and mechanical properties are shown in Table 2 and 3 [3, 4]. The general requirement of tensile strength limits as specified in ASME CODE (1989) is shown in Table 4. From the survey of current technical papers, there are three main aging mechanisms in aluminum 6061 alloy, that is, irradiation aging, corrosion and low cycle fatigue as discussed in the following.

1. Irradiation aging

Irradiation effects on aluminum alloys are relatively light. No drastic changes in mechanical properties and dimensional stability have been observed during tests in high flux research reactors. The threshold-integrated neutron fluences (both fast and thermal fluence) to cause aluminum alloy to loss of ductility was estimated to be in the order of 10^{12} n/cm^2 [4].

Aluminum has a transmutation cross section of $0.23 * 10^{-24}$ cm^2 for neutrons of .025 eV energy to produce silicon from the reaction $^{27}Al(n,\gamma)^{28}Al$, followed by the β decay to ^{28}Si [5, 6]. Irradiation with thermal neutrons triggers a novel phase instability in aluminum-based alloys. As such, a reactor with a relatively high thermal flux may readily produce 1% or more silicon by transmutation of aluminum atoms. Silicon is relatively insoluble in aluminum-based alloys, and in this case precipitated out as a fine dispersion of β' (Mg_2Si) particles as seen in Figure 4 [5]. The precipitates are believed to reduce void nucleation and growth by acting as sites for enhanced recombination of vacancies and interstitials and by retarding the climb of dislocations, which in turn reduces the rate at which dislocations absorb interstitials [5].

Farrell et al. [6], have studied the effects of irradiation of 6061-T6 aluminum in the High Flux Isotope Reactor (HFIR). They observed that the microstructure of the material from the unirradiated end of the hydraulic tube consisted of a very finely dispersed, acicular precipitate of Mg_2Si and the usual population of inclusions found in commercial alloys. There were also some isolated dislocations that were probably introduced after heat treatment during bending or straightening of the tube. Irradiation caused two obvious changes. One, it induced considerable precipitation of transmutation-produced silicon, especially heavy at grain boundaries. Elemental silicon is less dense than aluminum, 2.33 g /cm^3 versus 2.7 g /cm^3, and the introduction of precipitate of silicon causes the 6061 alloy to swell. The second change in the microstructure, observed only in material irradiated to fast fluences greater than $6 * 10^{22}$ n/cm^2, was the introduction of cavities. These cavities were heterogeneously distributed and not associated with the silicon particles, and they seemed to be absent from grain boundaries except at some inclusions that lay on the boundaries. There was no direct evidence that helium and hydrogen from (n,α) and (n,p) reactions were involved in fracture and ductility loss. The irradiation effects on tensile properties change are shown in Figure 5. Their results also show that, at a fast to thermal flux ratio of 0.6, a gradual increase in tensile strength and loss in ductility

begins at a fast (E > 0.1 MeV) fluence of 10^{21} n/cm^2, but that the ductility loss appears to saturate above a fast fluence of 10^{22} n/cm^2, as shown in Figure 6.

More recently, Weeks et al. [7, 8], studied the irradiation effects on 6061-T6 aluminum of control rod drive follower (CRDF) tubes in the High Flux Beam Reactor (HFBR) which is operated at a temperature of approximately 333 °k. Table 5 shows the summary data on HFBR irradiation of Al-6061-T6. Their results show that:

(1) The original Mg_2Si precipitates were replaced with a high concentration of 8 nm diameter, amorphous particles rich in silicon. The changes in mechanical properties are attributed to the development of the silicon-rich precipitates.

(2) 6061-T6 is a fully age-hardened alloy, it contains a massive network of internal sub-critical nuclei of magnesium silicide (Mg_2Si) so that little additional strengthening and loss in ductility were anticipated to be caused by fast neutrons. A high fast fluence may have the beneficial effect of randomizing the locations of the silicon atoms and therefore reducing their effects on mechanical properties of the alloy.

(3) Increase in tensile strength and decrease in ductility primarily from the thermal fluence. The higher the fast to thermal fluence ratio at the same thermal fluence, the less increase in tensile strength and the less decrease in ductility, as shown in Figure 7. Since, at high thermal to the fast fluence ratio will induce a high concentration of insoluble silicon per unit atomic displacement and, hence, a high degree of supersaturation and profuse nucleation of silicon-rich precipitates.

(4) The effects appear to be saturating at above approximately 1.8E23 n/cm^2 thermal fluence. The ductility appears to reach a minimum value of approximately 9%.

John Weeks et al. also proposed the equations that fit the experimental data for CRDF tubes tensile strength and elongation changes [8], as presented in the following.

$$T.S. = 50 + 24.5 * (\phi_{th} * 10^{-23})^{.5} \quad \text{in ksi, or}$$

$$= 345 + 170 * (\phi_{th} * 10^{-23})^{.5} \quad \text{MPa,}$$

$$\%\,E = 10.7 - 0.69 * (\phi_{th} * 10^{-23})$$

ϕ_{th} : Thermal Fluence in n/cm^2

2. Corrosion

Aluminum alloys have excellent corrosion resistance to air and water coolant (pure water and its vapor). The oxidation corrosion resistance of aluminum alloys lies in the fact that aluminum and oxygen have a high chemical affinity to form such oxides as Al_2O_3. The protective oxide film is tightly adherent on the metal surface that prevents or minimizes further attacks by free oxygen existing in most aqueous media.

Aluminum corrodes uniformly in the coolant water of thermal research reactors up to about 220 °C [4]. At higher temperatures, hydrogen atoms produced by the radiation decomposition and corrosion reaction

$$H_2O \rightarrow H + OH$$
$$2Al + 3OH \rightarrow Al_2O_3 + 3H$$
$$H + 3H \rightarrow 2H_2$$

diffuse into the metal and combine as molecular hydrogen. This can accelerate the corrosion rate during the development of corrosion products and gas blisters spread on the metal surface. Figure 8 [4] shows the typical corrosion curves of aluminum plate specimens exposed in water at various temperatures under atmospheric pressure.

The corrosion rate of aluminum as a function of pH has been relatively sparsely studied. The rate was found to depend logarithmically on the pH [26], different dependencies being noted on either side of the pH at which the corrosion is a minimum (close to 6). This value of pH is also close to that of the minimum solubility of various hydrated aluminas which may form as corrosive product films. Ambat et al. [27], studied the influence of pH on the corrosion of several aluminum alloys (not include Al-6061 alloy). Their results show that the corrosion rate is negligible for pH value between 5 to 8.

3. Low cycle fatigue

Y. S. Chung et al. [10], performed axial strain-controlled tests on five aluminum alloys (1200, 5083, 6061, 6351, and 7005) to provide information on their cyclic behavior. The experimental results are shown in Figure 9 and 10. They also conclude that the precipitation alloys, 7005, 6351, and 6061, show cyclic hardening followed by cyclic softening and the cyclic hardening generally increases with the strain amplitude and with the ratio of ultimate tensile stress to yield stress.

IV Evaluation of MITR--II Core Tank Suitability for Extended Operation

1. Irradiation aging consideration

As discussed in the section III, the primary concern of irradiation damage on MITR--II core tank is the degradation of structure integrity due to tensile properties change. There is no specific MITR--II core tank material (aluminum 6061 alloy) experimental data available to examine the mechanical properties change under irradiation. The formulas, proposed by Weeks et al., will be used to evaluate the suitability for extended operation of the core tank. The flux used in this calculation was obtained from 4-8-92 CITATION run [11]. Table 6 shows the corresponding flux information. The mesh point shown in the table refers to the core model in the John Bernard's thesis [12]. Figure 11, 12 and Table 7, 8, and 9 show the location and composition of each mesh points.

Since energy cutoff of the neutron flux in CITATION is not the same as those to be used in the formulas, the flux data from CITATION should be revised. The assumptions and formulas used in flux and fluence calculation are listed in the followings.

(1) MITR--II:

-- Accumulated fission energy as of 9-20-92 : 291,120.25 MWH [11].

-- Reactor operated at 4.9 MW, 200 days per year, during 9-20-92 to 5-7-96.

(2) MITR--III:

-- Reactor operated at 10 MW, 300 days per year, 20 years operation.

(3) Flux level for MITR--III:

-- Two times that of MITR--II.

(4) Empirical formulas to evaluate fast flux ($E \geq 0.1$ Mev) and corrected thermal flux (2200 m/sec) from CITATION [14]:

$$\int_{0.1\text{Mev}}^{\infty} \Phi(E)dE = 2.25 * \int_{1\text{Mev}}^{\infty} \Phi(E)dE$$

$$\int_{3\text{Kev}}^{\infty} \Phi(E)dE = 3.04 * \int_{1\text{Mev}}^{\infty} \Phi(E)dE$$

$$\Phi_{th} = \frac{\sqrt{\pi}}{2} * \left(\frac{293.6}{313}\right)^{.5} * F$$

-- F: group 3 flux from CITATION
-- assuming 40 °C @ core tank
-- Φ_{th}: 2200 m/sec thermal flux

The elongation and tensile strength at the end of each year are summarized in Table 10. Figure 13, 14 show the trend of cumulative thermal and fast fluence, while Figure 15, 16 show the trend of the elongation and the tensile strength. The figures and the table also show the trend of the fluence and properties change at the maximum flux point of the core. This is proposed to be a reference case for more conservative estimation purpose. The thermal to fast fluence ratio of MITR--II or III at core tank is approximately 1.8 which is well below the value of HFBR (Figure 7). The results should be conservative, assuming all others to be the same. The corresponding elongation and tensile strength at core tank after additional 20 years operation of MITR--III are 9.995 % E and 74.76 ksi, respectively. If the maximum flux of the core is used instead of flux at core tank, the elongation and tensile strength are 9.909 % E and 76.23 ksi, respectively. Although, the elongation is slightly smaller than specified 10 % E in ASME CODE (1989)* at the end of 20 years operation of MITR--III, operated at 10 MW, it is still well above 5 % E as recommended by John Weeks [15]. The 10 % limit in elongation in ASME CODE may be interpreted as an unirradiated limit but, this should be clarified.

* MITR Code compliance: ASME section II, 1968 (But, not available to the author up to the report time).

2. Corrosion consideration

The Al-Mg-Si (6000 series) alloys have excellent corrosion resistance in all natural atmospheric environment. As shown in Figure 8, at relatively low temperature, 200 °C to 250 °C, the corrosion rate is small and constant with exposure time. The operating temperature of MITR--II is 40 °C to 53 °C which is well below 200 °C. The pH value of the coolant system is in the range of 5.5 to 6.5 [1], which is around the value (6) for minimum corrosion rate as discussed in Section III. Therefore, the corrosion effect on the core tank material is negligible. Suppose the operating pressure, temperature and water chemistry of MITR--III are the same as that of MITR--II, there will be no corrosion damage on the core tank at the end of additional 20 years operation. However, this assessment is based on typical corrosion resistance characteristics of aluminum alloys, due to lack of specific experimental data for Al-6061 alloy. The field inspection of the core tank to determine the actual corrosion rate is strongly recommended. Besides, the environment of the reflector tank is quite different from that of the core tank, the corrosion rate at the

reflector tank should be examined separately. (Note: No corrosion evidence of the reflector tank was found, based on visual inspection conducted by MITR staff in 1989 [30].)

3. Fatigue consideration

For simplicity, the following formulas [23] are used to evaluate the stress level of the core tank.

$$\sigma \text{ (Pressure stress)} = \frac{P*R}{t}, \quad (\frac{R}{t} = 40, \text{ thin wall formula applicable})$$

$$\sigma_{th} \text{ (Thermal stress)} = \frac{E*\alpha}{1-\nu} * \frac{\Delta T}{2}$$

P : Pressure = 0.1 MPa
R : Core tank radius = 10 inches, at core region
t : Core tank thickness = 0.25 inches
α : Linear thermal expension coefficient = $23.4*10^{-6}/°C$
ν : Poisson's ratio = 0.28
E : Modulus of elasticity = $6.693*10^{4}$ MPa
ΔT : 50 °C (for conservative evaluation)

The total stress level of the core tank is approximately 60 MPa (neglect discontinuity stress, bending stress and other local factor, if any). As shown in Figure 10, the endurance limit [24] (i.e., the stress level which the material can withstand for an indefinite number of cycles without failure) of aluminum 6061 alloy is approximately 200 MPa. There is, at least, a factor of 3 for the core tank stress level to reach the endurance limit.

V Conclusions and Recommendations

1. Irradiation effects on aluminum alloys are relatively light. No drastic changes in mechanical properties and dimensional stability have been observed during tests in high flux research reactors.
2. Increase in tensile strength and decrease in ductility are primarily from the thermal fluence; that is , transmutation of aluminum to silicon. The higher the fast to thermal fluence ratio at the same thermal fluence, the less increase in tensile strength and the

less decrease in ductility.

3. The elongation at core tank after 20 years operation of MITR--III is slightly smaller than specified 10 % E in ASME CODE, but, it is still well above 5 % E as recommended by John Weeks. The 10 % limit in elongation in ASME CODE may be interpreted as an unirradiated limit but, this should be clarified.
4. The mechanical property tests of the core tank material, removed from MITR--II at the end of licensed operation lifetime, are recommended, if possible, to demonstrate the integrity of the core tank can be maintained during the lifetime of MITR--III.
5. Since CITATION code may not properly predict flux peak at the core interface regions, it is desirable that more precise flux map be provided so as to reduce the uncertainty in the core tank lifetime prediction.
6. The corrosion effect on the core tank structure integrity will be negligible, assuming the same water chemistry for MITR--III. However, the assessment is based on typical corrosion resistance characteristics of aluminum alloys, due to lack of specific experimental data for Al-6061 alloy. The field inspection of the core tank to determine the actual corrosion rate is strongly recommended.
7. There will be negligible cyclic fatigue effect on the core tank, assuming the same operating pressure and temperature for MITR--III.

References

1. MITR Staff, " Safety Analysis Report for the MIT Research Reactor (MITR-II)," 1970.
2. ASME CODE Section II, 1989.
3. William F. Smith, " Structure and Properties of Engineering Alloys," 1981.
4. Benjamin M. Ma, " Nuclear Reactor Materials and Applications," 1983.
5. K. C. Russell, " Phase Stability Under Irradiation," Progress in Materials Science Vol. 28, 1984.
6. K. Farrell and A. E. Richt, " Postirradiation Properties of the 6061-T6 Aluminum High Flux Isotope Reactor Hydraulic Tube," ASTM STP 570, 1975.
7. John R. Weeks, Carl J. Czajkowski, and Paul R. Tichler, " Effects of High Thermal and High Fast Fluences on the Mechanical Properties of Type 6061 Aluminum on the HFBR," ASTM STP 1046, 1990.
8. John R. Weeks, Carl J. Czajkowski, and Paul R. Tichler, " Effects of High Thermal Neutron Fluences on Type 6061 Aluminum," to be published in 1993.
9. Information Provided by Professor D. D. Lanning.
10. Y. S. Chung and A. Abel, " Low Cycle Fatigue of Some Aluminum Alloys," ASTM STP 942, 1988.
11. Personal Communication with K. Kwok, MITR Staff, 9-25-92.
12. John A. Bernard, Jr., " MITR-II Fuel Management, Core Depletion, and Analysis: Codes Developed for the Diffusion Theory Program Citation," M.S. Thesis, MIT Department of Nuclear Engineering, 1979.
13. E. F. Sturcken, " Irradiation Effects in Magnesium and Aluminum Alloys," Journal of Nuclear Materials 82, 1979.
14. Susan E. Best, " Characterization of the MIT Research Reactor for Fusion Reactor Related Studies," M. S. Thesis, MIT, 1979.
15. Personal Communication with John Weeks, BNL, 10-23-92.
16. M. Victoria, W. V. Green and D. Gavillet, " Nucleation and Growth of Precipitates and Helium Bubbles in a High-Purity A1-Mg-Si Alloy Irradiated with 600 MeV Protons," Journal of Nuclear Materials 155-157, 1988.
17. King, R. T., Jostsons, A., and Farrell, K., " Neutron Irradiation Damage in a Precipitation-Hardened Aluminum Alloy," ASTM STP 529, 1973.
18. S. Abis, et. al., " Investigation of Mg2Si Precipitation in an A1-Mg-Si Alloy by Small Angle Neutron Scattering," Journal of Nuclear Materials 135, 1985.
19. T. Kino , et. al., " Effects of Solute Atoms on the Evolution of Structural Damage in

Ion Irradiated High-Purity Aluminum Alloys," Journal of Nuclear Materials 155-157, 1988.

20. B.N. Singh , et. al., " Effects of 600 MeV Proton Irradiation on Nucleation and Growth of Precipitates and Helium Bubbles in a High-Purity A1-Mg-Si Alloy," Journal of Nuclear Materials 141-143, 1986.
21. F. King, " Aluminum and Its Alloys," 1987.
22. S. P. Carfagno and R. J. Gibson, " A review of Equipment Aging Theory and Technology," EPRI NP-1558, 1980.
23. Course 22.314J Class Notes.
24. S. H. Crandall, N. C. Dahl, and T. J. Lardner, "An Introduction to the Mechanics of Solids," 1978.
25. " Corrosion in Natural Environments," ASTM STP-558, 1974.
26. M. R. Tabrizi et al., " The Long-Term Corrosion of Aluminum in Alkaline Media," Corrosion Science, Vol. 32, 1991.
27. R. Ambat, E. S. Dwarakadasa, " The Influence of pH on the Corrosion of Medium Strength Aerospace Alloys 8090, 2091 and 2014," Corrosion Science, Vol. 33, 1992.
28. Z. Szklarska-Smialowska, " Insight into the Pitting Corrosion Behavior of Aluminum Alloys," Corrosion Science, Vol. 33, 1992.
29. E. Horn and H. Diekmann, " Corrosion of Aluminum and Aluminum Alloys in Nitric Acid," ASTM STP 1134, 1991.
30. Reflector Tank Inspection Result, MITR Procedure 7.6.1, Provided by MITR Staff, 11-30-92.

Figure 1 VIEW OF M.I.T RESEARCH REACTOR, MITR-II, SHOWING MAJOR COMPONENTS AND EXPERIMENTAL FACILITIES

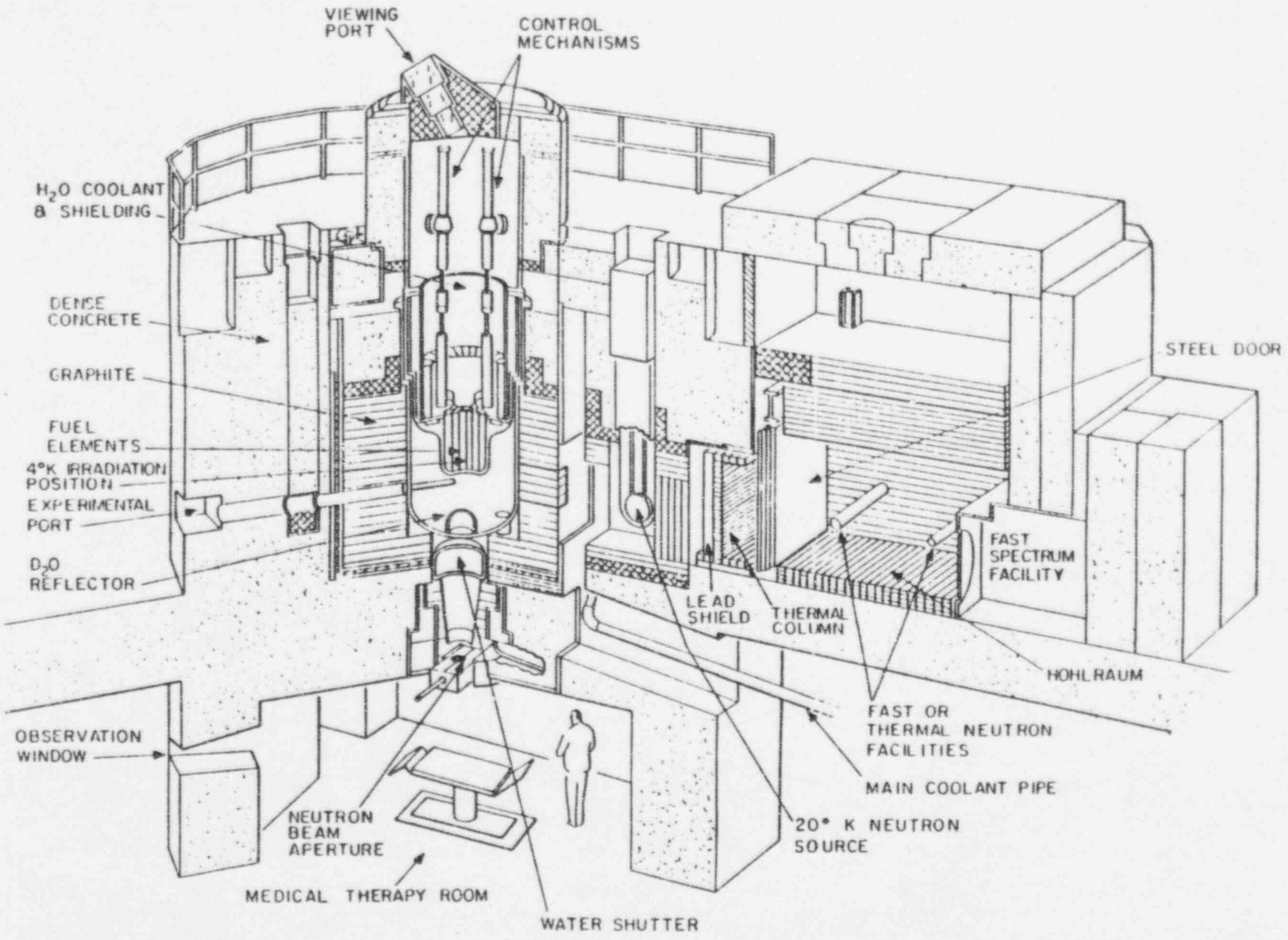

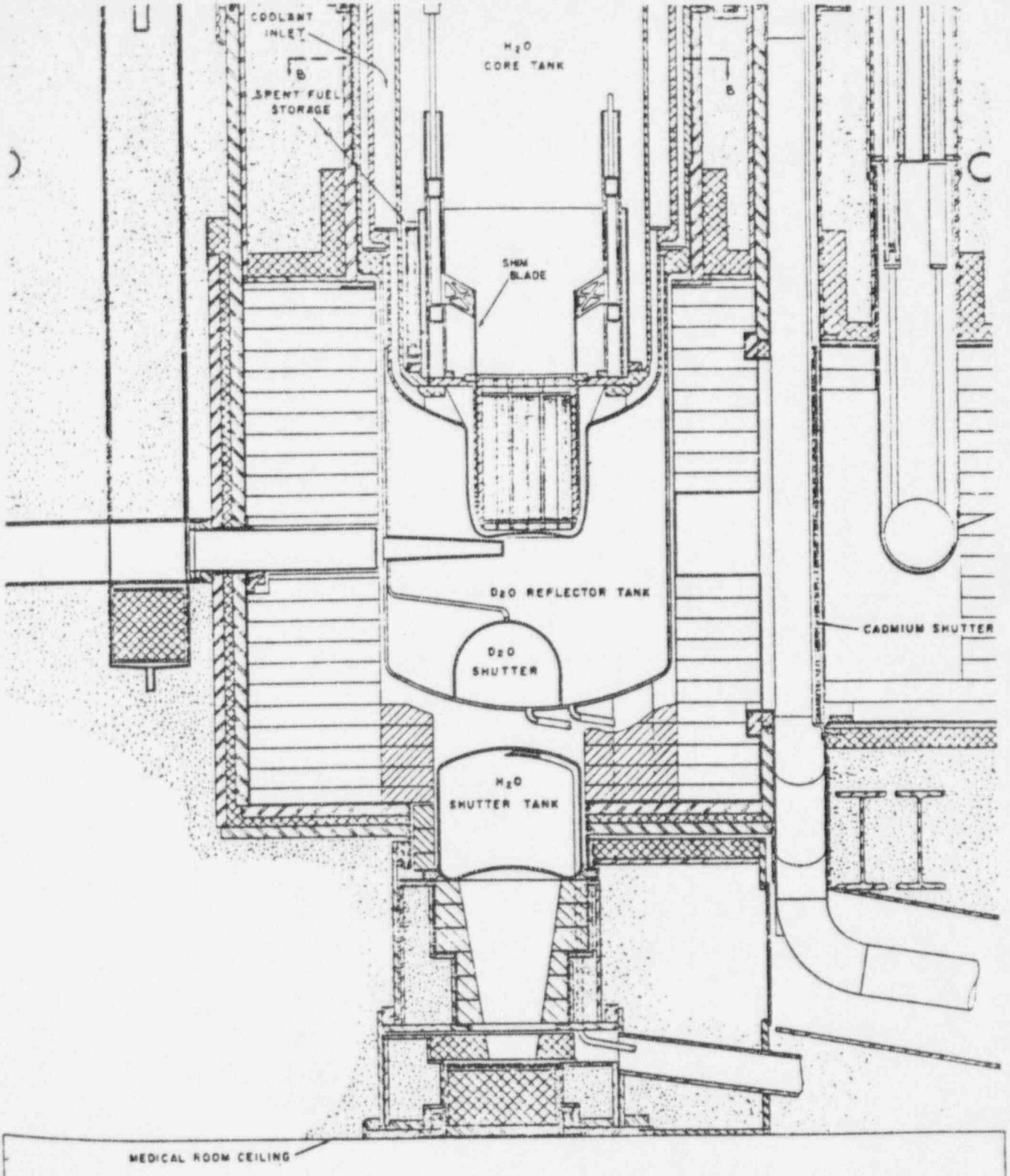

Figure 2 VERTICAL CROSS-SECTION MITR II

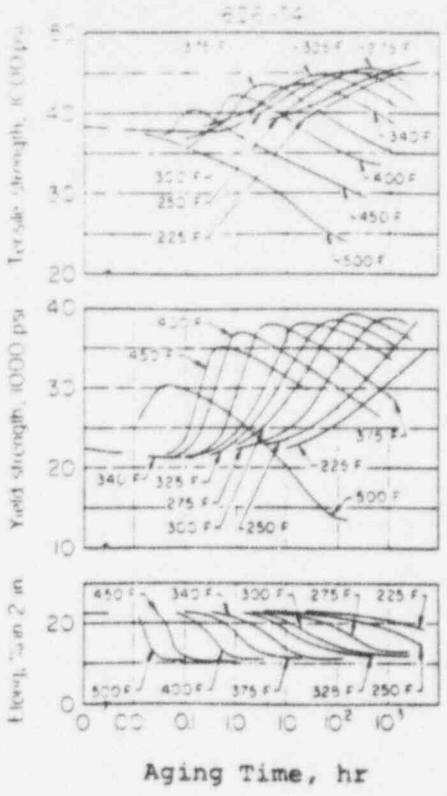

Figure 3 Aging characteristics of 6061 aluminum alloy [3].

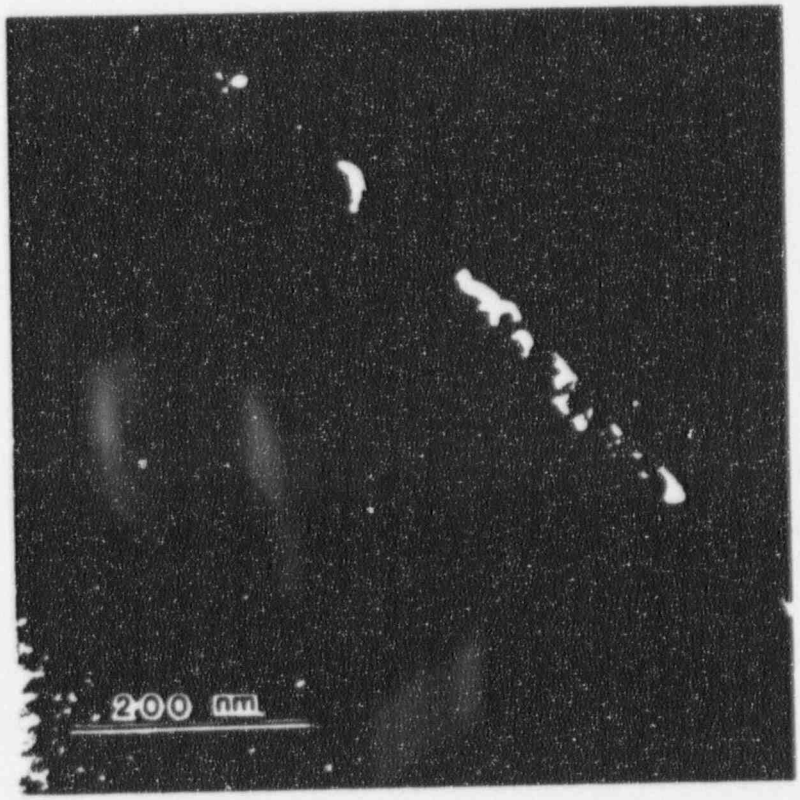

Figure 4 Dark field micrograph of precipitate reflections showing Mg_2Si precipitation at grain boundary and in grains [5]

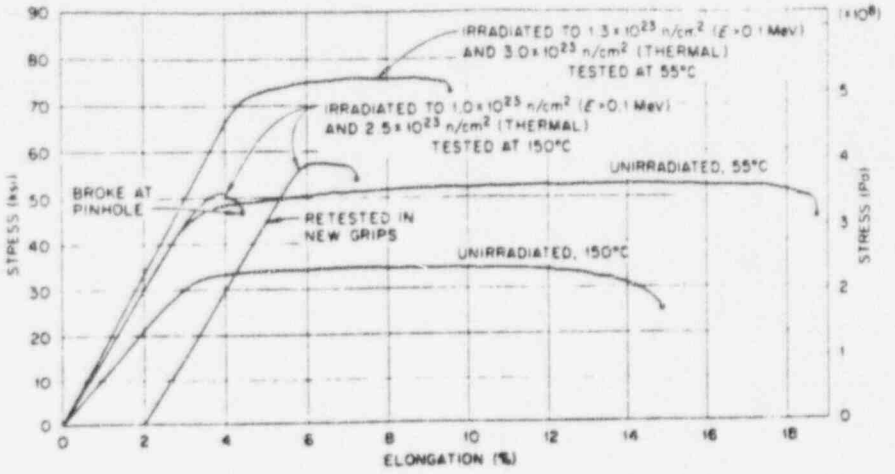

Figure 5 *Tensile curves at two temperatures* [6]

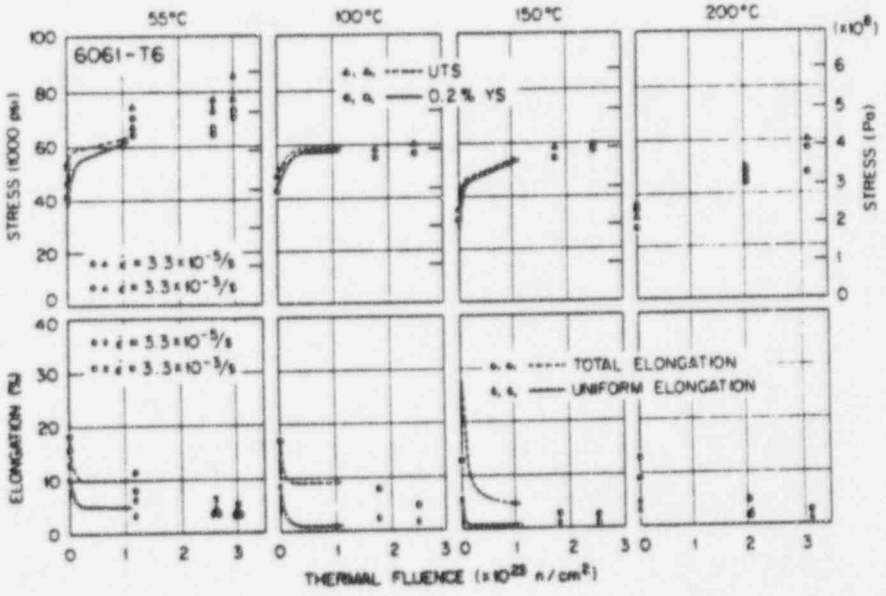

Figure 6 *Tensile properties of the irradiated and defilmed HFIR hydraulic tube at two strain rates and four test temperatures. The curves represent data from regular 6061-T6 surveillance specimens; the points are for the hydraulic tube. The thermal-to-fast fluence ratio is about 2.5 for the hydraulic tube specimens and about 1.3 for the surveillance specimens* [6]

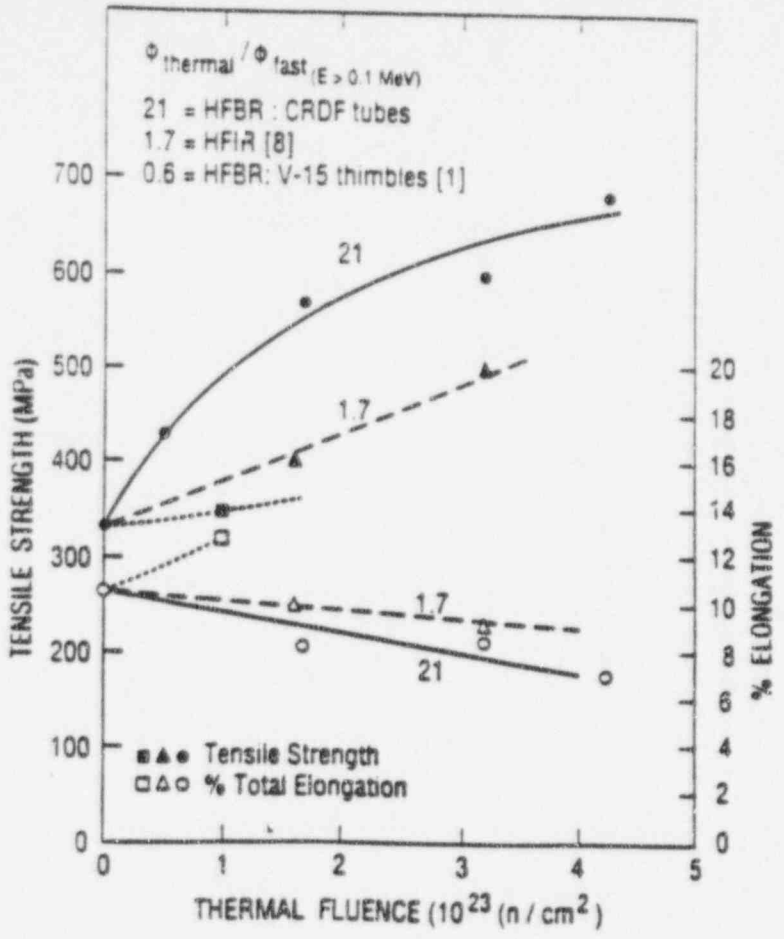

Figure 7 Effect of thermal to fast flux ratio on the mechanical properties of type 6061 T-6 aluminum.

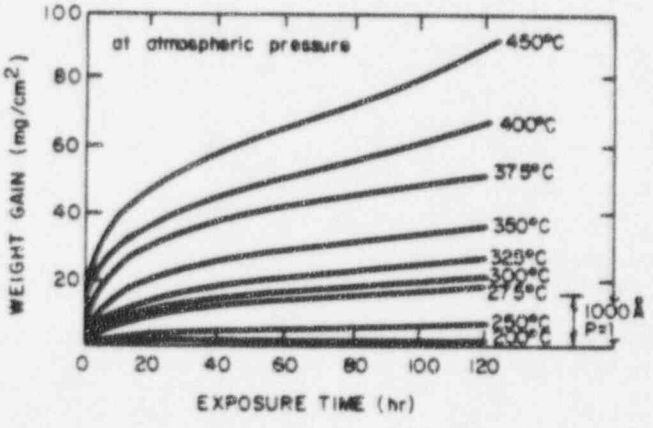

Figure 8 Typical corrosion curves for weight gain of aluminum exposed in water at various temperatures [4]

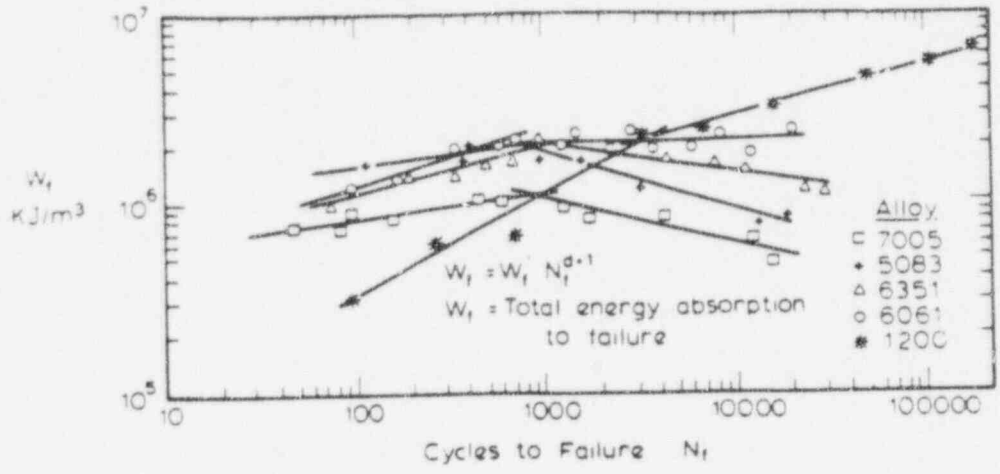

Figure 9 Total plastic energy versus fatigue life [10].

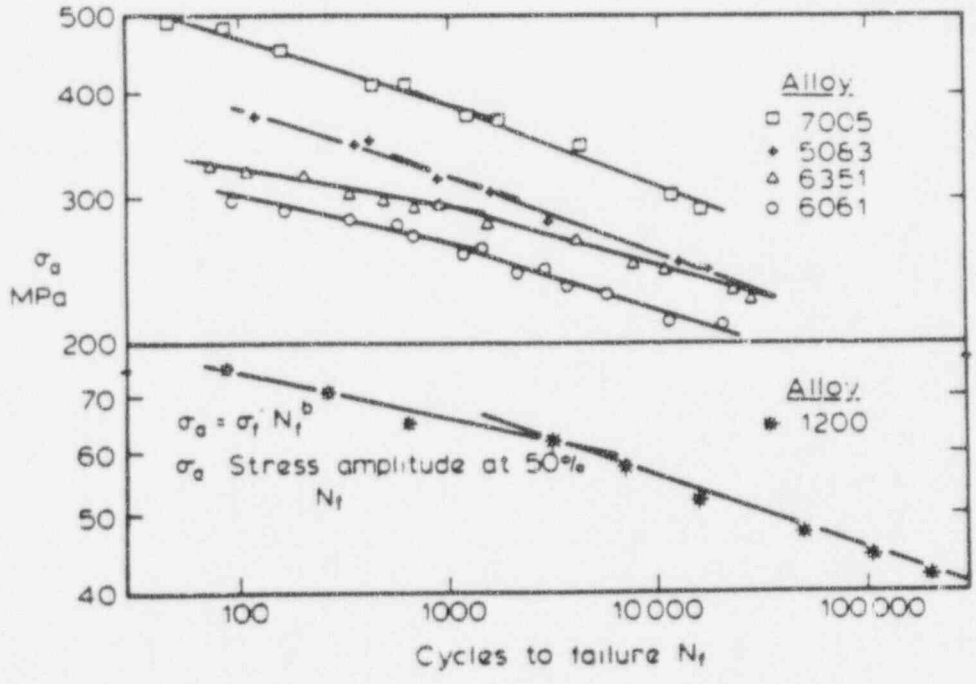

Figure 10 Stress amplitude versus fatigue life [10].

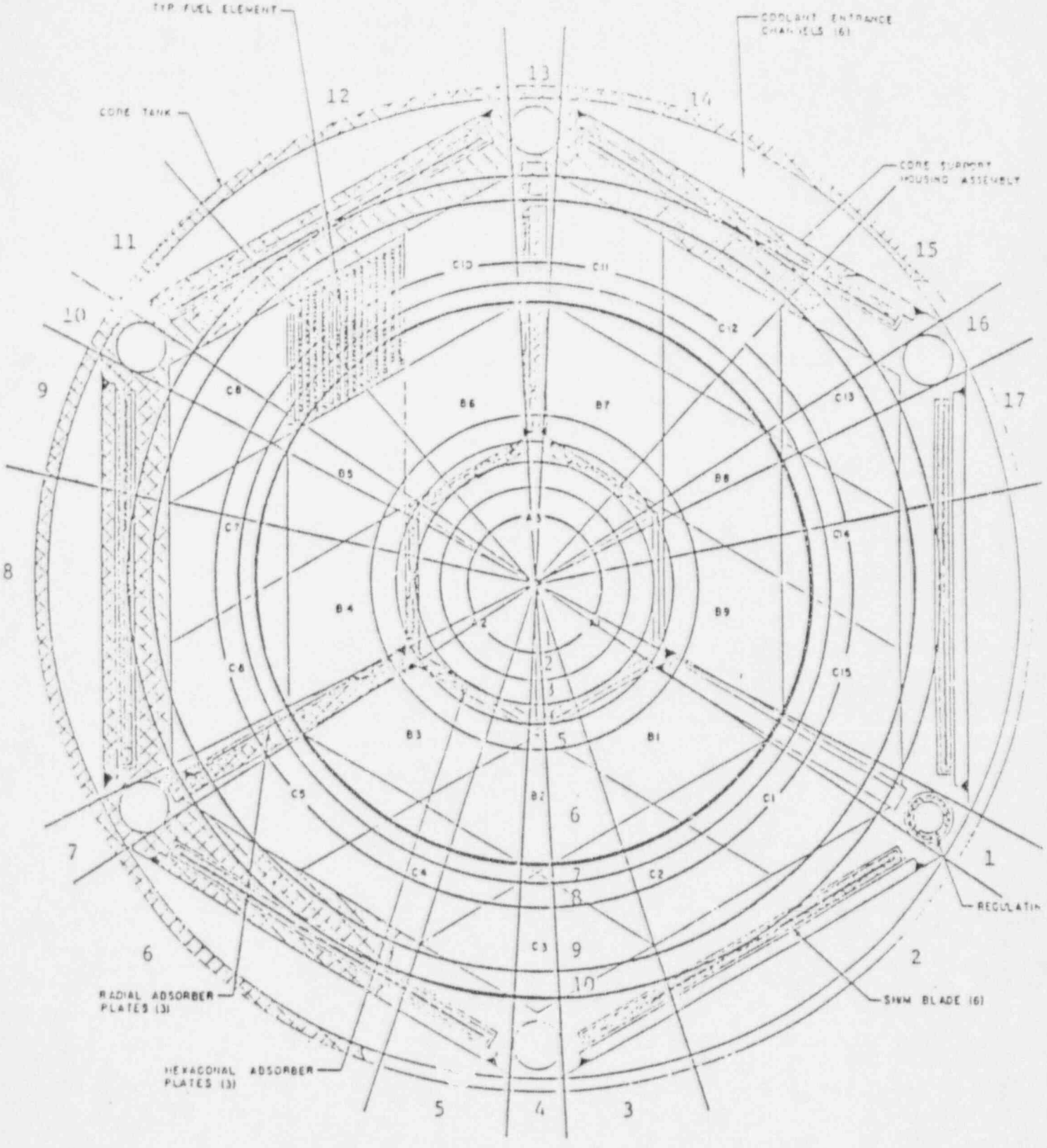

Figure 11 RADIAL AND AXIAL MESH: STANDARD MODEL

CORE SECTION MITR II

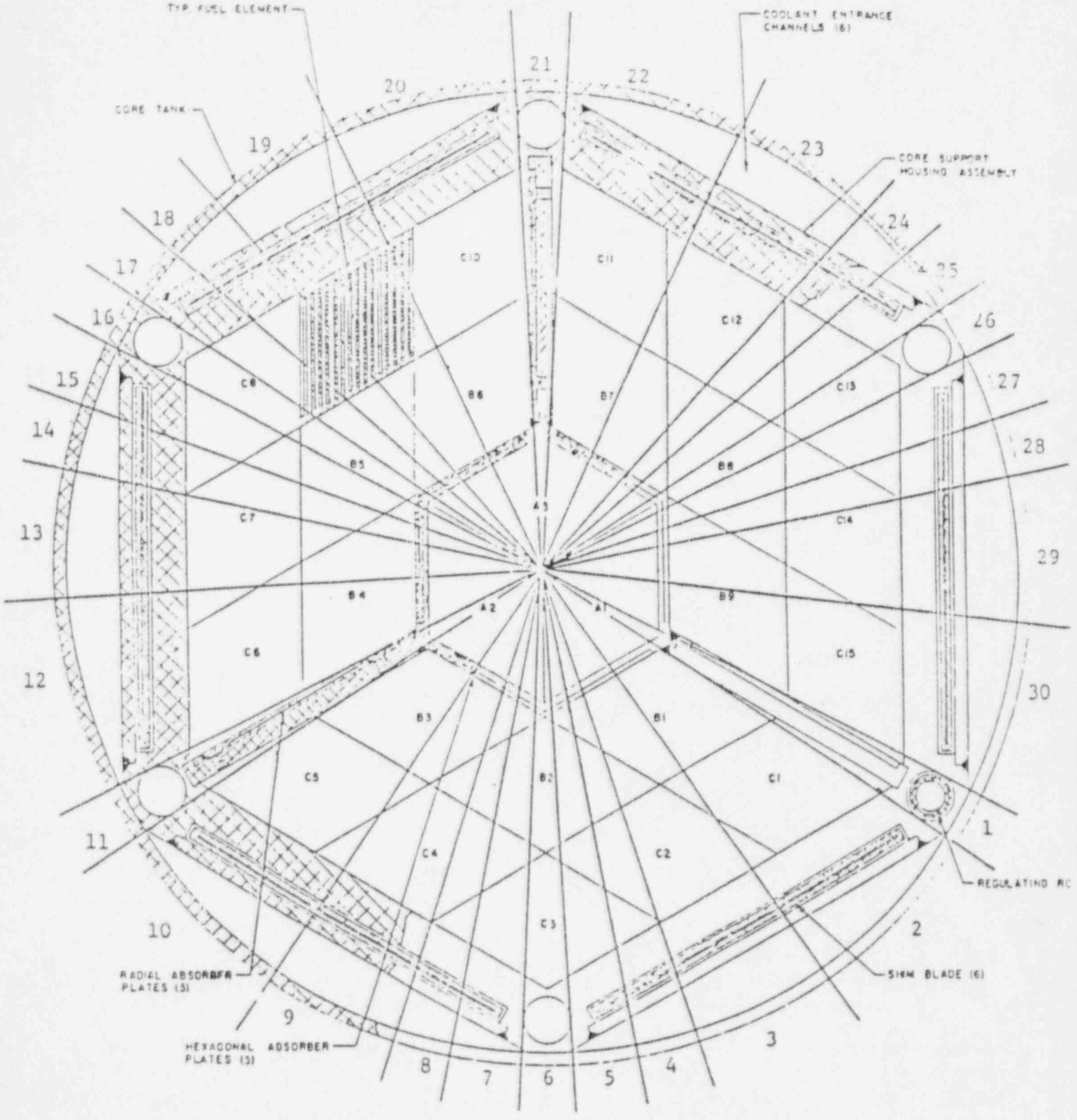

Figure 12 AZIMUTHAL MESH: ENLARGED MODEL

CORE SECTION MITR II

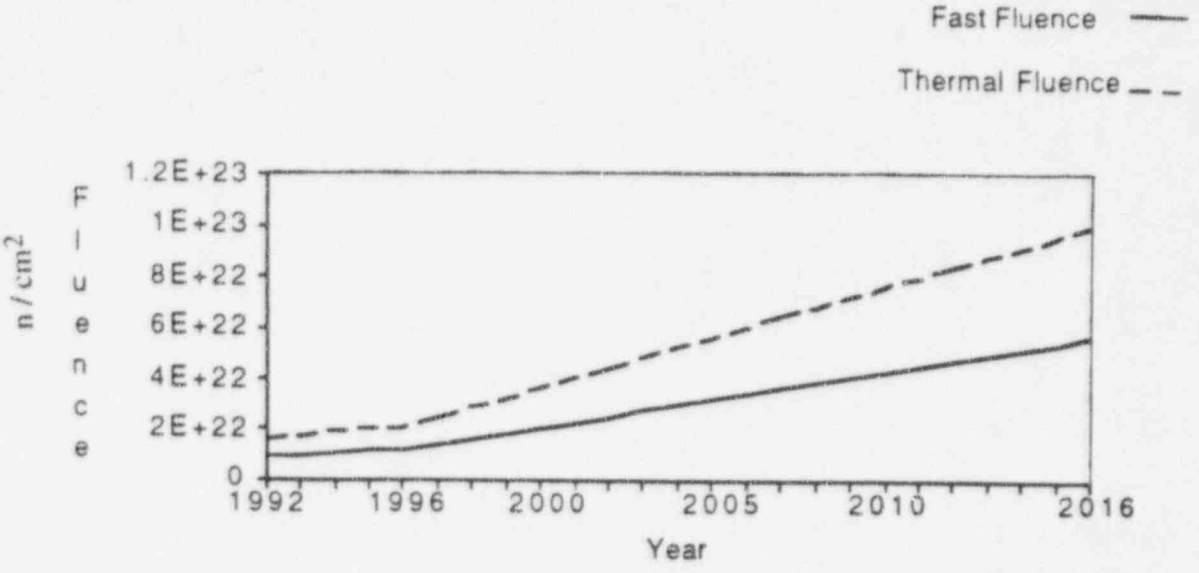

Figure 13 Thermal and fast fluence at core tank.

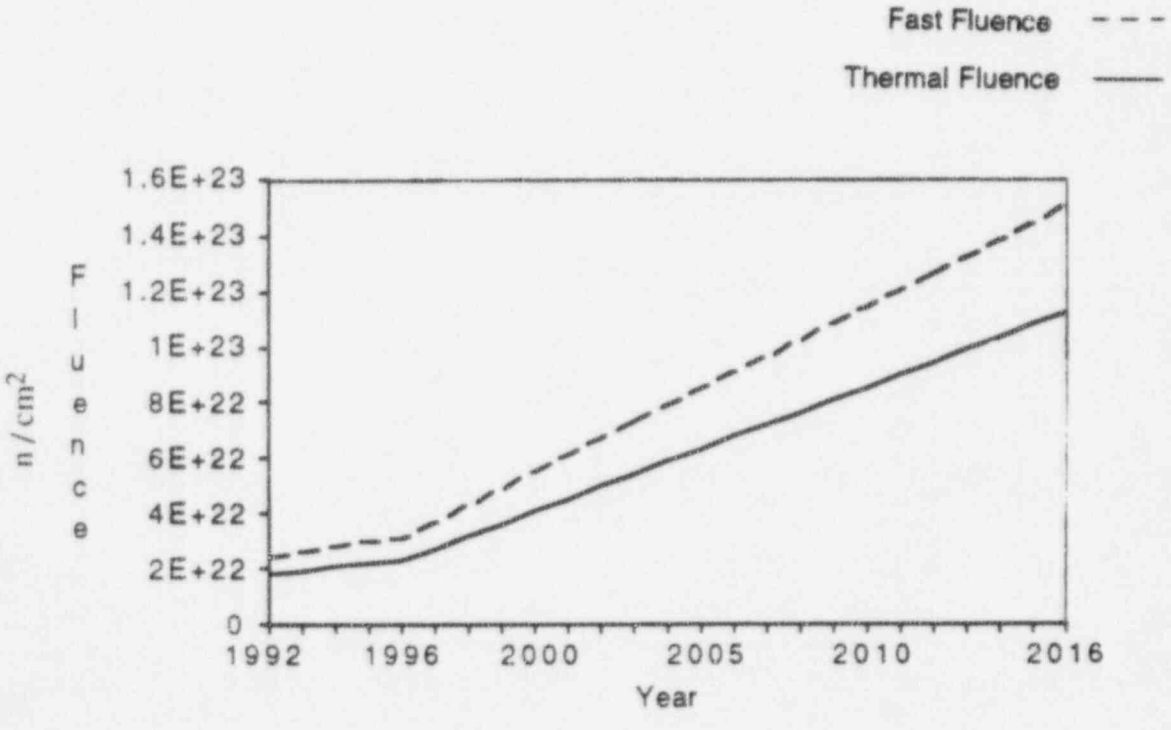

Figure 14 Core maximum thermal and fast fluence.

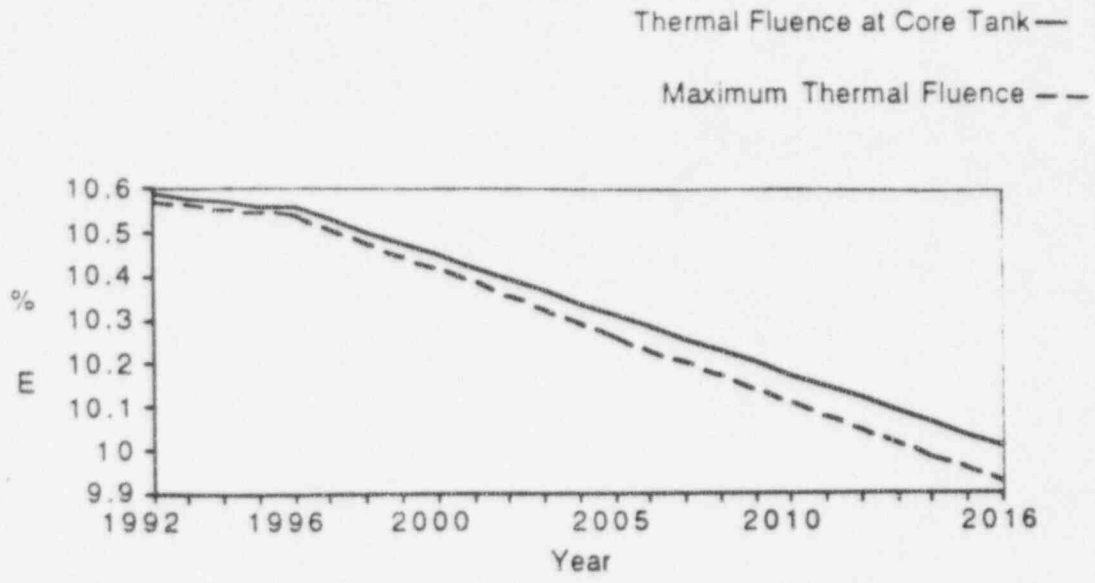

Figure 15 Reduction in ductility (% Elongation).

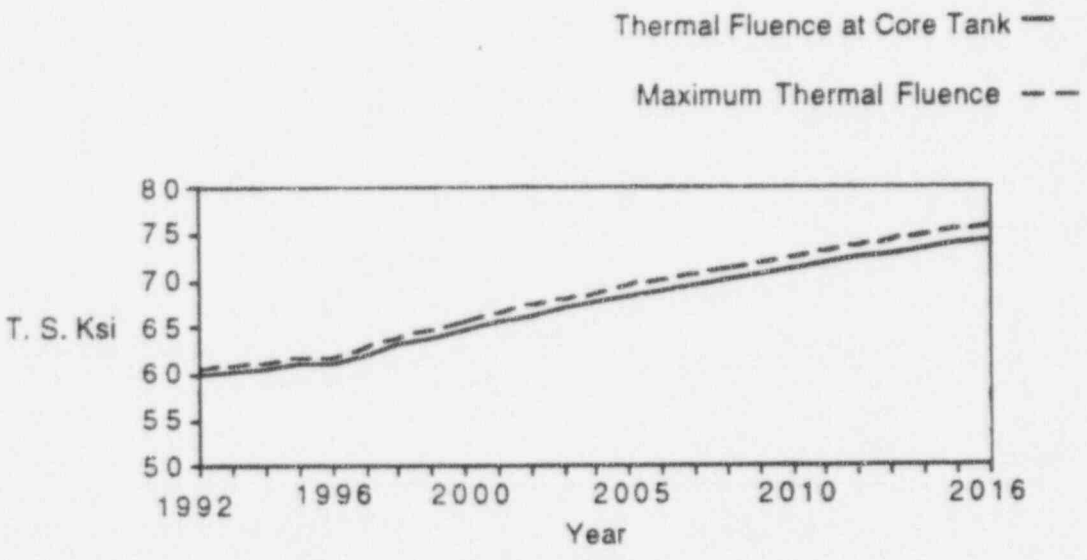

Figure 16 Increase in tensile strength.

Table 1 6061 ALUMINUM ALLOY CHEMICAL COMPOSITION LIMIT (ASME CODE)

Si	Fe	Cu	Mn	Mg	Cr	Zn	Ti	OTHER	Al
.4-.8	.7	.15-.4	.15	.8-1.2	.04-.35	.25	.15	.15	remainder

Table 2 Typical mechanical properties of wrought heat-treatable aluminum-magnesium-silicon alloys† [3]

Alloy	Temper	Tensile strength, psi	Tensile yield strength,‡ psi	Elongation, % in 2 in	Hardness, Bhn§	Shear strength, psi	Fatigue limit psi¶
6053	O	16,000	8,000	35	26	11,000	8,000
	T6	37,000	32,000	13	80	23,000	13,000
6061	O	18,000	8,000	25	30	12,000	9,000
	T4, T451	35,000	21,000	22	65	24,000	13,000
	T6, T651	45,000	40,000	12	95	30,000	14,000
	T81	55,000	52,000	15	...	32,000	
	T91	59,000	57,000	12	...	33,000	14,000
	T913	67,000	66,000	10	...	35,000	
6066	O	22,000	12,000	18	43	14,000	
	T4, T451	52,000	30,000	18	90	29,000	
	T6, T651	57,000	52,000	12	120	34,000	16,000
6070	O	21,000	10,000	20	35	14,000	9,000
	T6	57,000	52,000	12	120	34,000	14,000
6101	T6	32,000	28,000	15	71	20,000	...
6151	T6	48,000	43,000	17	100	32,000	12,000
6201	T81	48,000	...	6	...	...	15,000
6262	T9	58,000	55,000	10	120	35,000	13,000
6351	T4, T451	42,000	27,000	20	60	22,000	13,000
	T6, T651	49,000	43,000	13	95	29,000	13,000
6951	O	16,000	6,000	30	28	11,000	
	T6	39,000	33,000	13	82	26,000	

† After Ref. 1.
‡ Yield strength, 0.2 percent offset.
§ 500-kg load, 100-mm ball.
¶ Based on 500 million cycles using an R. R. Moore type of rotating-beam machine.

Table 3 Physical, Thermal, and Mechanical Properties of Aluminum and Its Alloys [4]

PROPERTY	Al AND Al ALLOY* Al	1100 (alloy)	6061 (alloy)	SAP (alloy)
Density 20°C (g/cm³)	2.699	2.71	2.70	2.7–2.8
Crystal lattice structure	FCC	FCC		
Lattice parameter, 20°C (Å)	4.049	4.050		
Melting point (°C)	660	645–655	620–650	>660
Boiling point (°C)	2060			
Specific heat, C_p 25–100°C (cal/g·°C)	0.226	0.230	0.230	
Thermal conductivity 25–100°C (cal/cm-sec-°C)	0.5035	0.52–0.53	0.52–0.53	0.40
Linear thermal expansion 20–100°C (10^{-6}/°C)	23.8	23.5	23.4	20
Ultimate strength				
annealed Al only (kg/cm²)	485	900–1680	900–2450	3500
cold-rolled (75%) Al (kg/cm²)	1120	(-0 -H18)	(o-T6)	
Yield strength (0.2 offset				
cold-rolled Al (kg/cm²)	1050	1500(-H18)	2100(-T6)	2500
Elongation annealed Al sheet only (%)	48.5	35 (-0)	25 (-0)	10 (rod)
cold-worked Al sheet (%)	5.5	5 (-H18)	12 (-T6)	
Modulus of elasticity 20°C 10^3 (kg/cm²)	700	700	710	710
Poisson's ratio	0.30	0.30	0.28	0.28
Hardness				
Brinell number cold-worked Al only	27	23–44	25–73	

*1100 Al alloy is commercially pure, 6061 Al alloy (0.7 w/o Mg, 0.4 w/o Si), SAP (7–14 w/o Al_2O_3).

Table 4 Tensile property limits [2]

Seamless Tube

Temper	Specified Wall Thickness,[b] in.	Tensile Strength, ksi min	Tensile Strength, ksi max	Yield Strength[c] (0.2% Offset) min, ksi	Elongation in 2 in. or 4 × Diameter,[f] min, % Full-Section Specimen	Elongation in 2 in. or 4 × Diameter,[f] min, % Cut-out Specimen
			Alloy 6061			
T4	0.025–0.049	30.0	...	16.0	16	14
	0.050–0.259	30.0	...	16.0	18	16
	0.260–0.500	30.0	...	16.0	20	18
T6	0.025–0.049	42.0	...	35.0	10	8
	0.050–0.259	42.0	...	35.0	12	10
	0.260–0.500	42.0	...	35.0	14	12

Plate

Temper	Specified Thickness, in.	Tensile Strength, ksi min	Tensile Strength, ksi max	Yield Strength (0.2% offset), ksi min	Yield Strength (0.2% offset), ksi max	Elongation in 2 in. or 4 × Diameter min, %
			Alloy 6061			
T4	0.051–0.249	30.0	...	16.0	...	16
T451[c]	0.250–1.000	30.0	...	16.0	...	18
	1.001–3.000	30.0	...	16.0	...	16
T6	0.051–0.249	42.0	...	35.0	...	10
T651[c]	0.250–0.499	42.0	...	35.0	...	10
	0.500–1.000	42.0	...	35.0	...	9
	1.001–2.000	42.0	...	35.0	...	8
	2.001–4.000	42.0	...	35.0	...	6
	4.001–6.000	40.0	...	35.0	...	6

Table 5 Summary of data on HFBR irradiation of Al-6061-T6 [7].

Source	Fluence, n/cm²: E > 0.1 MeV	Fluence, n/cm²: Thermal	Tensile strength, ksi	Percent Elongation, total	Number of Specimens
Alcoa Handbook	0	0	45	17	
Chow & Jones	0	0	48.4 ± 2.0	17.5 ± 2.5	2
ORNL	0	0	50.8 ± 0.6	11.0 ± 1	3
Czajkowski	0	0	47.8 ± 1	10.3 ± 0.5	4
Surveillance	5×10^{19}	2.7×10^{20}	48.2 ± 1.8	15 ± 1.0	2
Surveillance	2×10^{20}	1.07×10^{21}	50.4 ± 0.4	17.0	2
Surveillance	1.2×10^{21}	6.4×10^{21}	61.0 ± 3.0	12	2
CRDF A-6	7.9×10^{20}	1.7×10^{21}	82.7 ± 2.3	8.2 ± 1.6	4
CRDF A-7	2.2×10^{21}	4.9×10^{21}	62.3 ± 1.8	20.7 ± 0.7	7*
CRDF A-8	1.5×10^{22}	3.2×10^{22}	86.5 ± 8	8.6 ± 2	6
(A-8, ignoring lowest sample)			(88.3 ± 2.8)	(9.0 ± 0.3)	(5)
V-15.13"^	1.9×10^{22}	1.5×10^{23}	71.6 ± 1.2	10.2 ± 0.7	2
V-15.17"^	9.3×10^{22}	1.2×10^{23}	62.0 ± 0.4	11.6 ± 1.4	2
V-15.23"^	1.6×10^{23}	9.2×10^{22}	50.8 ± 2	12.9 ± 1.1	2
V-15.28"^	1.9×10^{23}	1.0×10^{23}	55.2 ± 0.8	15.7 ± 1.9	2

* Chow and Jones also include data from four specimens from the upper end of the tube, which contained little induced activity, indicating a much lower thermal fluence. These data were omitted from this evaluation.

^ Inches from top of vertical thimble flow shroud.

' The same specimen gave low values of both tensile strength and percent elongation.

Table 6 Neutron flux from CITATION (4-8-92).

FLUX., GROUP / FLUENCE	GROUP 1	GROUP 2	GROUP 3
FLUX @core tank	5.869E13	3.352E13	9.092E13
FLUX max	1.557E14	6.249E13	1.021E14

* Energy cutoff (ev)

	upper energy	mean energy
Group 1	1E07	5.472E04
Group 2	3E03	3.464E01
Group 3	4E-1	1E-2

* FLUX @ core tank : Maximum flux at core tank

* FLUX max : Maximum flux of the core

* Location of the flux (mesh point): R: Radial; Θ: Azimuthal; Z: Axial

- Core tank : Group 1: R15; Θ26; Z11
  Group 2: R15; Θ26; Z11
  Group 3: R15; Θ24; Z12
- Core max.: Group 1: R6; Θ27; Z11
  Group 2: R2; Θ2; Z11
  Group 3: R17; Θ26; Z11

Table 7 MITR-II AXIAL MESH: STANDARD MODEL

Mesh Interval (cm)	Location
30.48	Upper Water Plenum
10.16	Grid Plate
2.54	Fuel/Boron-Stainless Inserts
2.54	Fuel/Boron-Stainless Inserts
5.08	Fuel/Boron-Stainless Inserts
5.08	Fuel
5.08	Fuel
5.08	Fuel
5.08	Fuel
5.08	Fuel
5.08	Fuel
5.08	Fuel
5.08	Fuel
2.54	Fuel
2.54	Fuel
1.30	Lower Grid
0.60	Core Structure/Primary Coolant
1.90	Core Tank
3.20	Heavy Water/Aluminum
0.60	Light Water/Heavy Water
8.225	Heavy Water/Reentrant Beam Ports
46.645	Heavy Water Reflector

Table 8 MITR-II RADIAL MESH: STANDARD MODEL

Mesh Interval (cm)	Location
3.552	Inner A-Ring
0.896	Middle A-Ring
1.893	Outer A-Ring
0.634	Hexagonal Spider
1.000	Inner B-Ring
5.200	Middle B-Ring
1.000	Outer B-Ring
1.000	Inner C-Ring
3.282	Middle C-Ring
1.000	Outer C-Ring
0.9525	Core Housing
1.080	Regulating Rod
0.635	Control Blades
0.9525	Core Structure/Primary Coolant
0.681	Core Tank
1.721	Heavy Water Reflector
15.435	Heavy Water Reflector
15.435	Heavy Water Reflector
68.030	Reflector Tank/Graphite Reflector

Table 9 MITR-II AZIMUTHAL MESH: ENLARGED MODEL

Mesh Interval (radians)	Location
0.104790	A1, Radial Spider, Regulating Rod
0.397921	A1, B1, C1
0.265281	A1, B1, C2
0.132640	A1, B2, C2
0.146566	A1, B2, C3
0.104790	A2, B2, C3
0.146566	A2, B2, C3
0.132640	A2, B2, C4
0.265281	A2, B3, C4
0.397921	A2, B3, C5

Repeat the above sequence for the remaining two triads of the MITR-II core.

Table 10 Summary of data.

Year	ϕ_f @ core tank	ϕ_f core max.	ϕ_{th} @ core tank	ϕ_{th} core max.	% E @ core tank	% E core max.	T.S. ksi @core tank	T.S. ksi core max.
1992	9.2871E+21	2.4634E+22	1.6688E+22	1.8739E+22	10.5848523	10.5707023	60.0085045	60.605642
1993	1.0023E+22	2.6585E+22	1.801E+22	2.0223E+22	10.5757335	10.560463	60.397251	61.0175824
1994	1.0758E+22	2.8536E+22	1.9331E+22	2.1707E+22	10.5666148	10.5502236	60.7719774	61.414666
1995	1.1493E+22	3.0487E+22	2.0653E+22	2.3191E+22	10.557496	10.5399843	61.1340991	61.798393
1996	1.18E+22	3.13E+22	2.1203E+22	2.3809E+22	10.5536965	10.5357179	61.2815532	61.9546446
1997	1.4051E+22	3.7272E+22	2.5249E+22	2.8352E+22	10.5257819	10.504373	62.3108536	63.0453563
1998	1.6303E+22	4.3244E+22	2.9295E+22	3.2894E+22	10.4978673	10.4730281	63.2604975	64.0516587
1999	1.8554E+22	4.9216E+22	3.334E+22	3.7437E+22	10.4699527	10.4416832	64.1465356	64.9905605
2000	2.0806E+22	5.5188E+22	3.7386E+22	4.198E+22	10.4420381	10.4103383	64.9802585	65.8740258
2001	2.3057E+22	6.116E+22	4.1431E+22	4.6523E+22	10.4141235	10.3789934	65.7699658	66.7108494
2002	2.5308E+22	6.7132E+22	4.5477E+22	5.1065E+22	10.3862089	10.3476485	66.5219701	67.5077206
2003	2.756E+22	7.3104E+22	4.9523E+22	5.5608E+22	10.3582943	10.3163036	67.2412056	68.2698679
2004	2.9811E+22	7.9075E+22	5.3568E+22	6.0151E+22	10.3303797	10.2849587	67.9316158	69.0014701
2005	3.2063E+22	8.5047E+22	5.7614E+22	6.4694E+22	10.3024651	10.2536138	68.5964115	69.7059295
2006	3.4314E+22	9.1019E+22	6.1659E+22	6.9236E+22	10.2745505	10.2222689	69.2382483	70.3860601
2007	3.6565E+22	9.6991E+22	6.5705E+22	7.3779E+22	10.2466359	10.190924	69.8593523	71.0442211
2008	3.8817E+22	1.0296E+23	6.9751E+22	7.8322E+22	10.2187214	10.1595791	70.4616116	71.682413
2009	4.1068E+22	1.0894E+23	7.3796E+22	8.2865E+22	10.1908068	10.1282342	71.046644	72.3023502
2010	4.332E+22	1.1491E+23	7.7842E+22	8.7407E+22	10.1628922	10.0968893	71.6158484	72.905515
2011	4.5571E+22	1.2088E+23	8.1887E+22	9.195E+22	10.1349776	10.0655444	72.1704437	73.4931992
2012	4.7822E+22	1.2685E+23	8.5933E+22	9.6493E+22	10.107063	10.0341995	72.7115004	74.0665369
2013	5.0074E+22	1.3282E+23	8.9978E+22	1.0104E+23	10.0791484	10.0028546	73.239964	74.6265303
2014	5.2325E+22	1.388E+23	9.4024E+22	1.0558E+23	10.0512338	9.97150969	73.7566749	75.1740697
2015	5.4577E+22	1.4477E+23	9.807E+22	1.1012E+23	10.0233192	9.94016478	74.262384	75.7099509
2016	5.6828E+22	1.5074E+23	1.0212E+23	1.1466E+23	9.99540458	9.90881988	74.7577655	76.2348884

ϕ_f : Fast Fluence (n / cm^2), ϕ_{th} : Thermal Fluence (n / cm^2)

% E : % Elongation, T.S. : Tensile Strength in ksi

@ core tank : Max. Fluence at Core Tank

core max. : Max. Fluence of the Core